nature communications

Article

https://doi.org/10.1038/s41467-026-68537-7

Highly selective and practical hydrogenation of functionalized (hetero)arenes

Received: 24 April 2025

Accepted: 9 January 2026

Published online: 25 February 2026

Check for updates

Ruiyang Qu[1,2,8], Soumyashree Jena[1,8], Lifeng Xiao[3,8], Hui Yang[1,4,8], Rongsheng Cai[5], Stephan Bartling[1], Hanan Atia[1], Ralf Jackstell[1], Robert Franke[6,7], Kathrin Junge[1] ✉, Haijun Jiao[1] ✉, Graham J. Hutchings[3] ✉ & Matthias Beller[1] ✉

Arenes, and particularly heteroarenes are integral structural components of a variety of chemicals and represent a privileged class of bioactive compounds found in pharmaceuticals, agrochemicals and vitamins. Diastereoselective hydrogenation of multi-substituted (hetero)arenes offers an efficient and industrially relevant approach to convert these compounds into valuable, diversified 3D building blocks for applications for example in drug innovation. We show that a rationally designed Pt catalyst permits the general diastereoselective hydrogenation of a broad range of multi-substituted and functionalized arenes and heteroarenes using mild conditions. The corresponding cyclic products are obtained with very high diastereoselectivity (d.r. value up to 99/1). The practical applicability of this catalysis is illustrated by the straightforward preparation of a novel plasticizer on kg-scale under solvent-free conditions.

Arenes and heteroarenes are widely used in the chemical industry and are the most common structural motifs in small molecule pharmaceuticals, agrochemicals, and natural products[1]. They can be easily functionalized by various synthetic methods, making them versatile chemical intermediates for many products in our daily lives. Notably, the saturated (hetero)aromatic analogs are much less investigated compared with the well-explored (hetero)aromatic counterparts. To illustrate: Compared to aromatic acids/esters and the corresponding boronic acids/esters, cyclohexanecarboxylic acids/esters and cyclohexylboronic acids/esters are 1–3 orders of magnitude less commercially available (Supplementary Table 1). In contrast to their commercial availability, saturated (hetero)cycles have attracted rapidly growing attention in recent years in many fields such as the mass production of chemicals[2], energy generation[3], and storage[4,5], drug discovery[1], etc. Compared to the planar (hetero)aromatic compounds, their saturated (hetero)cyclic analogs have three-dimensional structures, especially when two or more substituents are present. This three-dimensionality of the structures offers the possibility of achieving significant positive changes in the compound properties. In the polymer industry, for example, the glass transition temperature (T_g) of a material can be adjusted by manipulating the ratio between *cis* and *trans* diastereomers[2]. A number of other examples can be found in current drug research. Here, there is a growing interest in the integration of more three-dimensional structural components and the use of sp^3-C centers in the development of new drugs ("escape from the flatland") in order to improve the diversity of bioactive compound libraries and expand the chemical space[6–8]. Indeed, beneficial correlations have been demonstrated between increased molecular complexity and the improved clinical success of compound transition from discovery to drugs[9]. As a consequence, 3D-saturated (hetero)cyclic scaffolds are featured in a large number of top-selling small molecule drugs in recent years. However, it remains challenging and step-intensive to synthesize the desired multi-substituted (hetero)cyclic 3D scaffolds[10].

[1]Leibniz-Institut für Katalyse e.V., Rostock, Germany. [2]CHN Energy Europe Research GmbH, Berlin, Germany. [3]Cardiff Catalysis Institute School of Chemistry, Cardiff University, Cardiff, UK. [4]National Institute of Clean-and-Low-Carbon Energy, Beijing, China. [5]State Key Laboratory of Solid Lubrication, Lanzhou Institute of Chemical Physics, Chinese Academy of Sciences, Lanzhou, China. [6]Evonik Oxeno GmbH & Co. KG, Marl, Germany. [7]Lehrstuhl für Theoretische Chemie, Ruhr-Universität Bochum, Bochum, Germany. [8]These authors contributed equally: Ruiyang Qu, Soumyashree Jena, Lifeng Xiao, Hui Yang. ✉e-mail: Kathrin.Junge@catalysis.de; Haijun.Jiao@catalysis.de; hutch@cardiff.ac.uk; Matthias.Beller@catalysis.de

https://doi.org/10.1038/s41467-026-68537-7

Table 1 | Diastereoselective hydrogenation of dimethyl phthalate (1a)

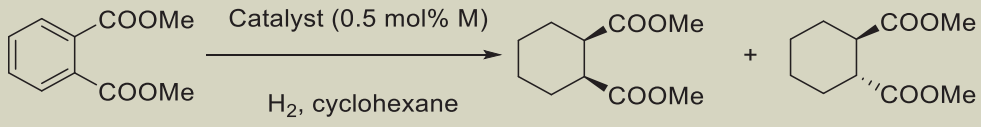

1a 2a 3a

Entry[a]	Catalyst	*T*/°C	*P*/bar	*t*/h	Conversion/%[b]	Yield/%[b]	d.r.[c]
1	Pd/C[d]	25	10	0.5	0	0	-
2	Ru/C[d]	25	10	0.5	0	0	-
3	Ni/C	25	10	0.5	0	0	-
4	Co/C	25	10	0.5	0	0	-
5	Cu/C	25	10	0.5	0	0	-
6	Pt/C[d]	25	10	0.5	13	12	99/1
7	Pt/C[e]	25	10	0.5	3	3	-
8	Pt/Al_2O_3	25	10	0.5	4	3	-
9	Pt/SiO_2	25	10	0.5	<1	<1	-
10	Pt/TiO_2	25	10	0.5	23	23	99/1
11	Pt/TiO_2	25	10	16	>99	98	99/1
12	Pt/TiO_2	60	10	16	>99	99	99/1
13	Pt/TiO_2	120	10	16	>99	97	99/1
14	Pt/TiO_2	25	1	16	>99	98	99/1

T reaction temperature, *P* H_2 pressure, *t* reaction time.
[a]Reaction conditions: dimethyl phthalate (0.5 mmol), [M] (0.5 mol%), cyclohexane (2 mL).
[b]Determined by GC-FID using *n*-hexadecane as an internal standard, average of two runs.
[c]Diastereoisomeric ratio (d.r.) corresponding to the *cis* product calculated by GC-FID, average of two runs.
[d]Commercial catalyst supplied from Sigma Aldrich.
[e]Commercial catalyst supplied from Strem Chemicals.

Among the numerous known synthetic methods for the preparation of aliphatic saturated (hetero)cyclic compounds, catalytic stereoselective hydrogenations are probably the most general, powerful, and atomically efficient method[11]. In this respect, diastereoselective hydrogenations offer a direct pathway to unlock the 3D chemical structures starting from abundant 2D (hetero)arenes with di- or multi-substituents. However, the high kinetic barrier to break aromaticity (e.g., the aromatic stabilization energy for benzene is 36 kcal·mol^{-1})[12] and to achieve chemo- and stereoselectivity in the presence of other functional groups remain major challenges for any catalyst development. Nevertheless, sophisticated molecular catalysts including borenium-[13], borane-[14,15], iridium-[16], rhodium-[17–20], zirconium-[21], and molybdenum-based complexes[22] allowed to achieve such transformations. From a practical point of view, homogeneous systems have intrinsic disadvantages like more difficult catalyst recycling, sensitivity, often complex ligand synthesis, and/or the use of basic or acidic additives. Obviously, the development of a robust heterogeneous catalyst is more attractive for many applications, especially on a larger scale. Despite the many heterogeneous catalysts developed for arene hydrogenations[3,4,23–26], there is only a very limited number of publications regarding the diastereoselective hydrogenation of multiple-substituted (hetero)arenes, and most known materials make use of chiral auxiliaries[27,28] or Lewis acids[29].

Following today's vision of increasing sustainability in advanced chemical production, we herein present a unique heterogeneous Pt catalyst, which allows for the general diastereoselective hydrogenation of a variety of multi-substituted (up to six substituents!) and functionalized (hetero)arenes under mild reaction conditions. A combination of kinetic studies and modern characterization techniques identified a two-shell Pt structure as the most active site. To showcase the practicability of the catalyst and methodology, a phthalate-free plasticizer (*cis*–1,2-cyclohexanedicarboxylic acid, dioctyl ester) was prepared on a kg-scale under solvent-free conditions.

Results and discussion

Material synthesis and kinetic investigations of the benchmark system

As a model reaction, the diastereoselective hydrogenation of the industrial bulk product dimethyl phthalate (**1a**, DP for short) to provide dimethyl 1,2-cyclohexane dicarboxylate was used, as the related higher esters are of interest as an alternative for phthalate plasticizers. To achieve high stereoselectivity and to identify highly active materials, catalytic tests were performed under mild reaction conditions (25 °C, 10 bar H_2 pressure).

We commenced the study testing different commercially available and homemade supported metal catalysts (Table 1). Except for Pt-based catalysts, which showed limited conversions, no activity was observed for all the other tested materials (Pd/C, Ru/C, Ni/C, Co/C, and Cu/C) under these conditions (Table 1, entries 1–7). Variation of the support showed Pt/TiO_2 as the optimal catalyst composition (Table 1, entries 6–10). For all the tested Pt/TiO_2 materials, an excellent diastereoselective ratio (d.r.) of 99:1 towards the *cis*-product (**2a**) was obtained in a wide temperature range from 25 °C to 120 °C (Table 1, entries 11–13), which is different compared to other Pt-based catalysts[30]. The ester group also remained intact, and no over-hydrogenation occurred[31]. With an increased reaction time, excellent yield and d.r. can be observed at ambient conditions (25 °C, 1 bar H_2 pressure, Table 1, entry 14). We also noted that, commercial Pt/C from different suppliers exhibited different activities (Table 1, entries 6 and 7). It is thus interesting and significant to identify the real catalytically active site to allow reproducible material preparation and the rational design of a highly efficient catalyst. Hence, we prepared a series of

https://doi.org/10.1038/s41467-026-68537-7

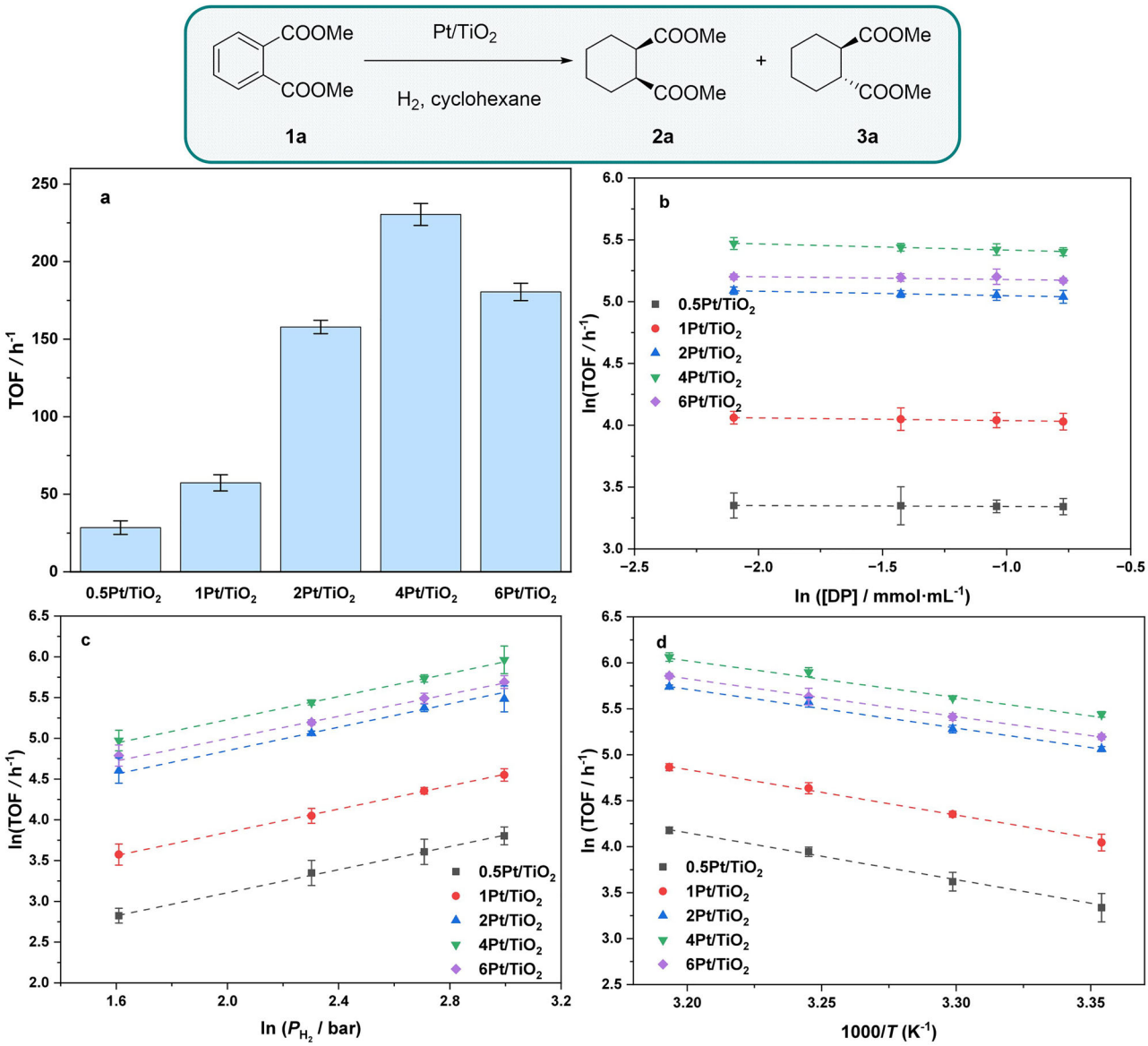

Fig. 1 | Activity tests and kinetic studies of Pt/TiO_2-catalyzed hydrogenation of 1a. a) The effect of Pt loading on the activity. **b** Reaction orders with respect to the substrate. **c** Reaction orders with respect to H_2. **d** Arrhenius plots. The error bars represent the standard deviation obtained from three independent performance tests. Reaction conditions: 0.25–1 mmol substrate, 0.5 mol% Pt, 5–20 bar H_2, 2 mL cyclohexane, 25–40 °C.

Pt/TiO_2 catalysts with different Pt loadings (denoted as xPt/TiO_2, where x represents the weight percentage of Pt) using an impregnation method as reported[32]. The measured Pt loading of all the prepared samples is very close to the designed value, as evidenced by the ICP-OES results (Supplementary Table 2). As shown in Fig. 1a, turnover frequency (TOF) shows an increasing trend when the Pt loading increases from 0.5 wt% to 4 wt%, followed by a slight decrease when further increasing the Pt loading to 6 wt%. To illustrate this phenomenon, kinetic studies were performed. The effect of mass transfer was eliminated (Supplementary Fig. 1) to ensure that the data were collected in a kinetically controlled region. The reaction orders for substrate **1a** and hydrogen are almost identical for all samples tested (Fig. 1b): an order close to 0 for **1a** and a positive order in the range of 0.7 ± 0.1 for hydrogen (Fig. 1c, data summarized in Supplementary Table 4). These reaction order values are consistent with those reported in the literature for the hydrogenation of benzene[33,34], toluene[35], and benzoic acid[36] over Pt-based catalysts. A zero-order reaction for **1a** indicates that the substrate **1a** is involved in the reaction in a strongly adsorbed state. In addition, the reaction order values measured here are supposed to reflect a reaction mechanism in which the hydrogen addition to the intermediate on the catalyst surface is most likely the rate-determining step of this reaction. While we should note that it is also possible that during the reaction, the catalyst surface is saturated with substrate **1a**, resulting in the hydrogen chemisorption as the kinetically limiting step. The effect of temperature on the reaction rates of all catalyst samples can be seen in the Arrhenius diagram (Fig. 1d). The dependencies in the Arrhenius diagram were linear in the investigated temperature range of 298–313 K for all investigated samples. Hence, the apparent activation energy (E_a) can be determined within this region. For all the samples, the E_a values are quite close, within the range of 33–42 kJ·mol^{-1}, which is in agreement with reported data[34,37]. The measured kinetic parameters, including the reaction orders for the substrate **1a** and H_2, together with the apparent activation energies, did not differ significantly for all the tested samples, suggesting no obvious change in the reaction mechanism. Consequently, we would consider that the difference in reactivity originates from the number of active sites. In other words, since the total number of Pt centers involved in the reaction is the same

https://doi.org/10.1038/s41467-026-68537-7

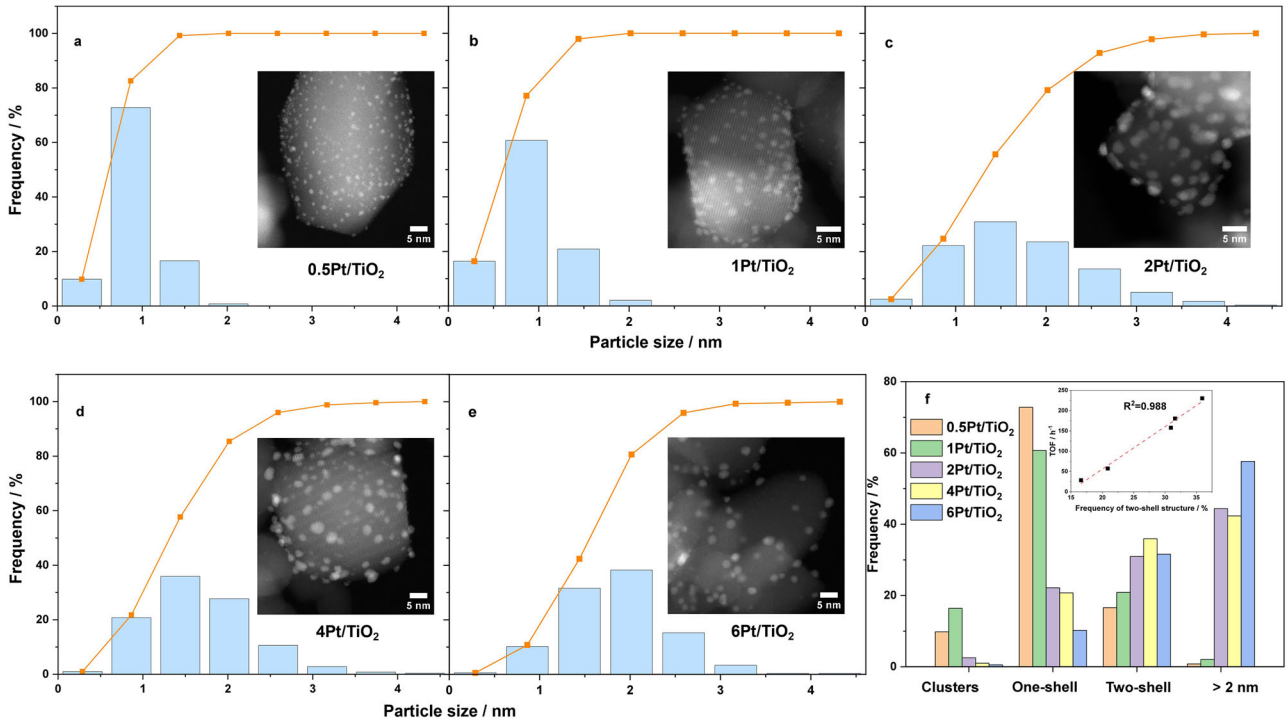

Fig. 2 | Representative HAADF–STEM images and the derived particle size distributions of the series of Pt/TiO_2 catalysts with different Pt loadings, categorized according to the physical model. a $0.5Pt/TiO_2$. **b** $1Pt/TiO_2$. **c** $2Pt/TiO_2$. **d** $4Pt/TiO_2$. **e** $6Pt/TiO_2$. **f** Relative populations of supported Pt clusters/NPs with different structures; Inset: the correlation between the frequency of two-shell structured Pt and TOF.

Table 2 | Calculated van der Waals diameter of dimethyl phthalate and model catalysts

	Dimethyl phthalate	One-shell Pt Pt_{13}/TiO_2	Two-shell Pt Pt_{55}/TiO_2	Three-shell Pt Pt_{159}
Structure model	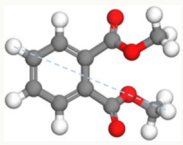	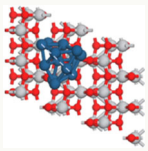	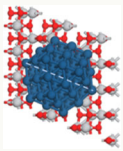	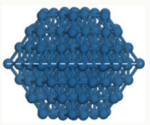
Measured distance/nm	0.79	0.53	1.05	1.74
Van der Waals diameter/nm	1.03	0.88	1.40	2.09

(0.5 mol%) for all samples, it is reasonable to assume that some specific centers are the most active sites for the reaction, while others are less active or even inactive.

Identification of catalytically active sites

The catalyst structure essentially comprises the electronic and the geometric structure[38]. To uncover the most active site of the catalyst, we first performed X-ray Photoelectron Spectroscopy (XPS) to explore the effect of the electronic structure on the reactivity. As shown in Supplementary Fig. 2, both Pt^0 and PtO were observed for all the samples. The fractions of these two species are quite close (around 62–66% for Pt^0 and 34–38% for PtO, as shown in Supplementary Table 5), indicating that the electronic structure is not the decisive factor for the difference in the catalytic reactivity. Therefore, we assume a determinant role of the geometric structure, although controversial conclusions have been drawn for the hydrogenation of benzene and toluene. Such reactions have been designated as structure-insensitive reactions by groups of Verykios[39] and Figueiredo[40], while Somorjai and co-workers[37] observed a moderate structure sensitivity for these hydrogenation reactions. To investigate the size distributions of supported Pt clusters and nanoparticles (NPs), we used scanning transmission electron microscopy (STEM). Some representative high-angle annular dark-field (HAADF) images are shown in Fig. 2a–e, which are categorized according to the physical model with different numbers of shells (definition is given in Supplementary Figs. 3 and 4 and Table 2)[32]. A significant amount of one-shell structured Pt was observed over $0.5Pt/TiO_2$ and $1Pt/TiO_2$. Because these two samples exhibited the least reactivity (Fig. 1a), we conclude that this type of Pt structure is not the most active site. When the Pt loading increases, the number of clusters (particle size < 0.5 nm) becomes negligible, while that of two-shell structured Pt and larger Pt NPs increases to some extent. Here, we summarize the relative populations of supported Pt with different structures. When the Pt NP are present in a three-shell structure or even larger size, its property becomes similar to the Pt(111) surface, which generally has a weak affinity to the substrate. For this reason, we have grouped these NPs together. As shown in Fig. 2f and the inset, a good correlation has been observed between the fractions of two-shell structured Pt and TOF, suggesting that such a type of Pt structure may be the most active Pt site for the reaction. To prove this hypothesis, we synthesized another

https://doi.org/10.1038/s41467-026-68537-7

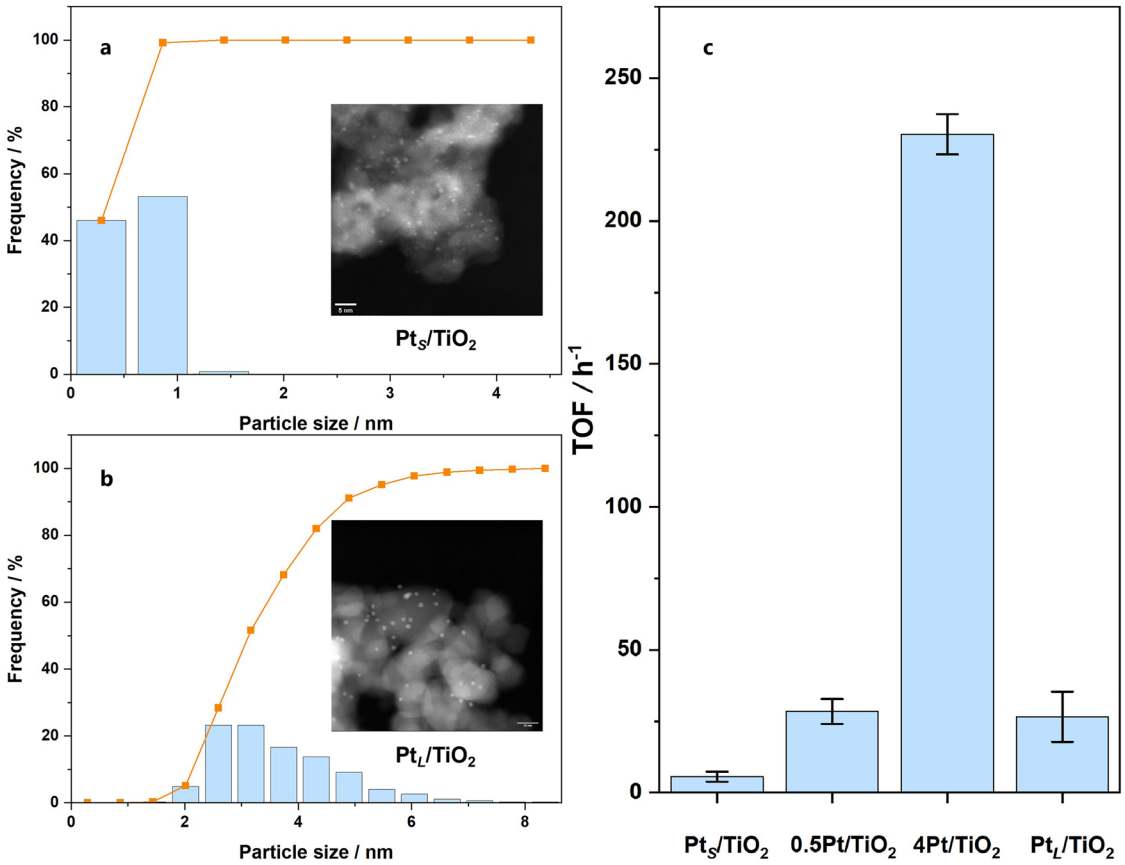

Fig. 3 | Representative HAADF–STEM images, the derived particle size distributions, and activity tests of the Pt_S/TiO_2 and Pt_L/TiO_2 catalysts. a Pt_S/TiO_2. **b** Pt_L/TiO_2. **c** Comparison of TOF with 0.5Pt/TiO_2 and 4Pt/TiO_2. The error bars represent the standard deviation obtained from three independent performance tests. Reaction conditions: 0.5 mmol substrate, 0.5 mol% Pt, 10 bar H_2, 2 mL cyclohexane, 25 °C, conversions and yields were determined by GC-FID using *n*-hexadecane as an internal standard.

two types of Pt/TiO_2 catalysts: (1) supported Pt clusters with almost all the Pt size below 1 nm (denoted as Pt_S/TiO_2, Fig. 3a) and (2) supported Pt NPs with Pt size > 2 nm (denoted as Pt_L/TiO_2, Fig. 3b). Both catalysts exhibited limited activity, with reaction TOF even lower than that of 0.5Pt/TiO_2 (Fig. 3c). These results strongly suggest that the two-shell structured Pt is most likely the most active site for this reaction.

Density functional theory (DFT) calculations were performed to illustrate the size compatibility between the catalyst and substrates. The van der Waals diameter of **1a**, calculated to be 1.03 nm (Table 2 and Supplementary Table 6), is larger than the size of a one-shell structured Pt nanoparticle (0.88 nm). Since H_2 molecules should also dissociatively adsorb on Pt sites, it is natural to conclude that the size of this one-shell Pt nanoparticle (or even smaller Pt cluster) is too small to accommodate both **1a** and H_2 concurrently. The surface site will be over-covered by **1a** based on the rather strong adsorption energy (−2.28 eV, Supplementary Table 7) on Pt_{13}/TiO_2. This might explain the very limited reactivity observed over the small-sized Pt catalyst. However, once the Pt size is too large, the adsorption of **1a** on the Pt surface becomes much weaker (−0.63 eV for three-shell Pt_{159} and −0.21 eV for Pt(111) surface, see Supplementary Table 7), and this is contrary to our kinetic analysis, which shows that **1a** was involved in the reaction in a strongly adsorbed state. Consequently, the two-shell structured Pt nanoparticle, which has a size of 1.40 nm (Table 2), is large enough to accommodate both **1a** and H_2 concurrently, and the adsorption energy of **1a** (−2.07 eV., Supplementary Table 7) indicates a strong adsorption, as found in our kinetic analysis. Therefore, both factors make the two-shell structured Pt the most active site for the diastereoselective hydrogenation of dimethyl phthalate.

Synthetic applications

After identifying the optimal Pt/TiO_2 catalyst in the benchmark reaction, we tested the hydrogenation of diverse substituted arenes and heteroarenes to evaluate the reaction scope and limitations (Fig. 4). Obviously, a broad substrate scope and functional group tolerance are prerequisites for advanced fine chemical applications. Substrates with substituents in the different positions of the arene ring were efficiently hydrogenated and gave very good to excellent yields and diastereoselectivities. By varying the position of the substituents in phthalates from *ortho, meta to para*, a slight decrease in diastereoselectivity is observed. While ortho-phthalates gave >99/1 diastereoselectivity, generating only a single diastereomer in quantitative yield (**2a**), the *meta*- and *para*-phthalates provided quantitative yields but lower selectivity (**2b**, **2c**). In all cases, the corresponding *cis*-isomers were produced preferentially. Notably, product **2d** was synthesized from n-octyl phthalate[41,42], a commercial plasticizer, using standard reaction conditions with >99% diastereoselectivity. Similar to phthalates, substituted benzoic acid esters with electron-donating or -withdrawing moieties, showed comparable reactivity and diastereoselectivity (**2e**–**2h**). Irrespective of the electronics of the substituents, *ortho*-substituted benzoates gave excellent diastereoselectivities. Furthermore, methyl 3,4-dimethyl benzoate provided **2i** in 90% isolated yield and a high d.r. value (92/8). Hydrogenation of ibuprofen methyl ester was performed at 60 °C using cyclohexane as solvent, which provided the corresponding hydrogenated product in 94% isolated yield (**2v**). In this case, the diastereoselectivity was comparable to other ester-containing arenes like **2g**, **2h**, and **2j**.

The diastereoselective hydrogenation of non-functionalized substrates and substrates with weakly coordinated functional groups is

https://doi.org/10.1038/s41467-026-68537-7

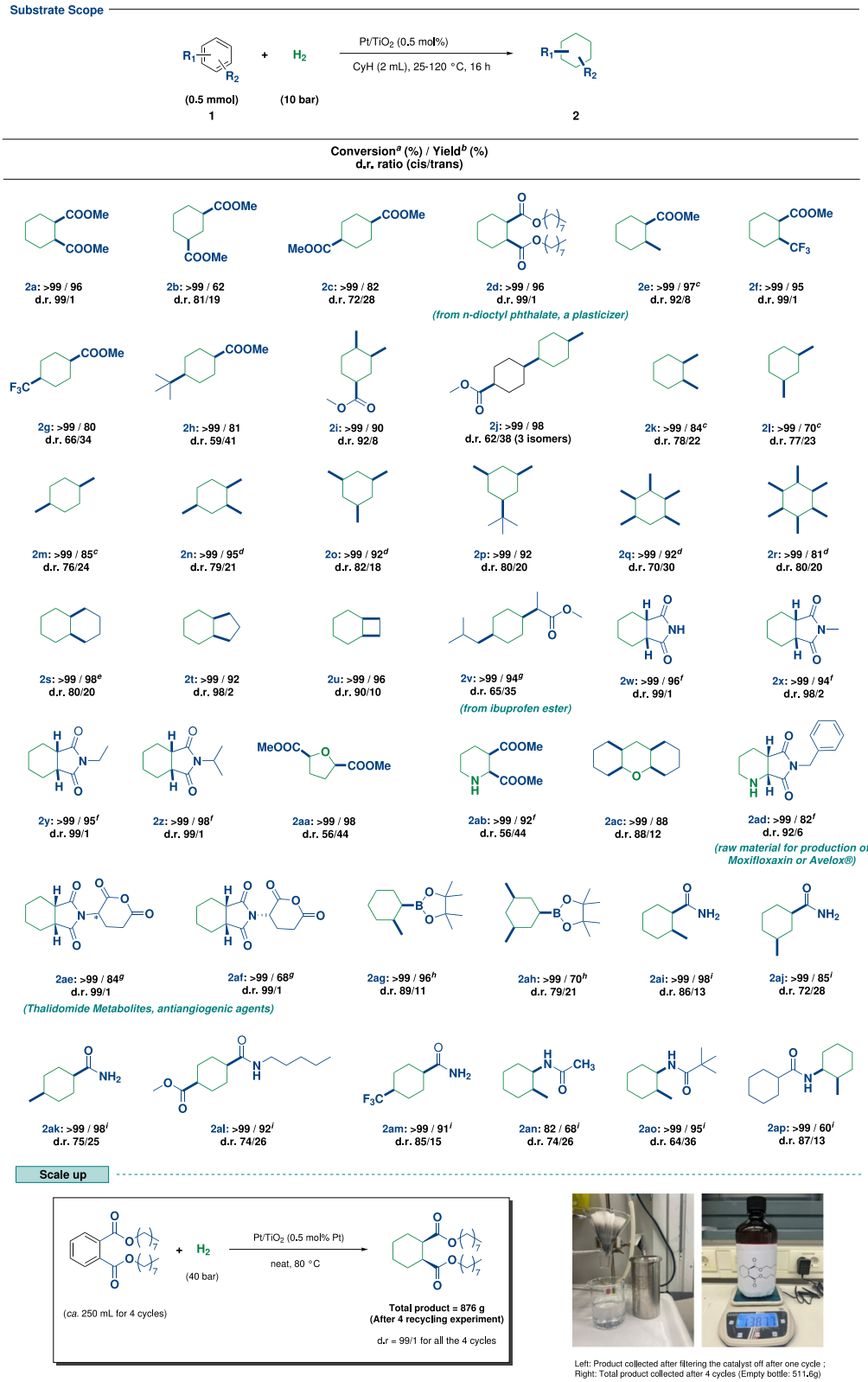

Fig. 4 | Synthetic applications and kg-scale synthesis of non-phthalate-based plasticizers.

considered an extremely challenging problem[43–45]. In contrast to starting materials that bind to the catalyst (center) via a strong interaction, the fundamental difficulty with such transformations is that a large number of transition states are feasible. Exemplarily, catalytic hydrogenation of xylenes was performed. Interestingly, in all the cases a similar d.r. Ratio (around 3:1) is obtained irrespective of the position of the second methyl group (**2k**–**2m**). In these cases, product yields were calculated based on ^{1}H NMR due to the lower boiling point of the corresponding 1,n-dimethylcyclohexanes or based on isolated products after filtering of the catalyst using neat conditions.

Next, we investigated some tri-substituted arenes under standard reaction conditions. Indeed, the products **2n**–**2p** formed with similarly

good diastereoselectivities compared to di-substituted arenes. Even tetra- and penta-substituted benzenes can be diastereoselectively (i.e., up to 80:20) hydrogenated to **2q**–**2r** with the Pt/TiO_2 catalyst system. As an example of fused-ring arenes, tetrahydronaphthalene was hydrogenated to form octahydronaphthalene (**2s**) in 98% GC yield and 80/20 d.r. value. Finally, bicyclic strained arenes were hydrogenated, providing **2t**–**2u** with excellent diastereoselectivities, too.

The stereoselective hydrogenation of heteroarenes offers an effective strategy for the direct access to saturated heterocycles. In recent years, several homogeneous[46–48] and heterogeneous[49–51] catalyst systems have been developed for such reductions with high levels of chemo- and stereoselectivity. However, using heterogeneous catalysts for this task remains a challenge. Hence, we investigated the hydrogenation of pyridine (**1ab**) and phthalimides (**1w**–**1z**) in the presence of water as solvent at 60 °C. While dimethyl pyridine-2,3-dicarboxylate was hydrogenated with moderate diastereoselectivity, in the case of phthalimides, the reaction was highly selective to generate one diastereomer in high isolated yields. Also, 6-membered heterocyclic 9*H*-xanthene provided both arene hydrogenated product (**2ac**) in very good d.r. The heterocyclic product **2ad** was also easily isolated with excellent diastereoselectivity after performing the hydrogenation reaction at 60 °C in water. **2ad** is an important building block in the synthesis of (4aS,7aS)−6-benzyloctahydro-1H-pyrrolo[3,4-b] pyridine, which is commonly used as a crucial intermediate in the preparation of the drug moxifloxacin[52–54]. Similarly, hydrogenation of isoindoline-1,3-dione derivatives, which constitute an important group of medicinal substances[55,56], provided the corresponding saturated heterocycles in excellent diastereoselectivities and with very good, isolated yields (**2ae**–**2af**).

Next, two examples of pinacol borane esters containing arenes with additional one and two substituents (**2ag**–**2ah**) were tested. While at room temperature, no conversion was observed, the corresponding hydrogenated products were provided with very good diastereoselectivity at 80 °C. Interestingly, substituted benzamides (**2ai**–**2ap**) formed the cyclohexanecarboxamides in good d.r. values, too. Compared to secondary amides, primary amides gave higher diastereoselectivity, while tertiary amides didn't show any reactivity even at higher reaction temperatures.

Reusability, stability, and easier separation of product and catalyst are intrinsic advantages of heterogeneous catalysts, as described at the beginning. For the model reaction, the Pt/TiO_2 catalyst shows a stable conversion (*ca.* 40%) and d.r. value (99/1) during 5 runs (Supplementary Fig. 5). STEM characterization of the recycled catalyst reveal that the proposed Pt structure basically holds, with a slight decrease in the fraction of one-shell NPs and a tiny increase in the proportion of larger particles (>2 nm) (Supplementary Fig. 6). In order to demonstrate the practicability of this catalyst system and the process described herein, the diastereoselective hydrogenation of di-n-octyl phthalate was performed on kg-scale. This reaction was selected due to the concerns about the toxicity of phthalates and the interest in developing alternative non-phthalate-based plasticizers in industry[2]. To examine its stability and recycling, the Pt/TiO_2 catalyst was recycled four times under neat conditions. The desired product was collected simply using filtration, without any further purification operations. 876 g of the *cis*-product was obtained with a d.r. value > 99:1 (Fig. 4).

In conclusion, we have developed a heterogeneous Pt catalyst allowing for the general diastereoselective hydrogenation of a wide range of (hetero)arenes under comparably mild conditions (10 bar H_2; 25–120 °C). Detailed characterizations and kinetic experiments revealed a two-shell Pt structure as the most active site, which opens up the possibility for further rational design of catalysts for diastereoselective hydrogenations. The kg-scale synthesis of a phthalate-free plasticizer demonstrates the potential of such transformations for industrial applications.

Methods

Catalyst preparations

TiO_2-supported Pt catalysts with different Pt loadings (0.5 wt%, 1 wt%, 2 wt%, 4 wt%, 6 wt%) were synthesized using the wet-impregnation method. For a typical catalyst preparation (0.5 g), the desired amount of aqueous hydrogen hexachloroplatinic acid solution (7.5 mg Pt·mL^{-1}, Alfa Aesar) was diluted to 16 mL using deionized water, and heated in an oil bath to 60 °C with vigorous stirring (800 r.p.m.) for 15 min, followed by the addition of TiO_2 support (P25, Sigma-Aldrich). The temperature was kept at 60 °C for 16 h. After being cooled down, water was removed using rotatory evaporation. The resultant material was then put into the oven at 110 °C overnight. The sample was ground thoroughly and then calcined at 450 °C for 4 h with a heating rate of 10 °C·min^{-1}. Finally, the sample was reduced in a flow-tube furnace under a steady flow of 5% H_2/Ar at 250 °C for 1 h with a heating rate of 5 °C·min^{-1}. This series of catalysts are denoted as xPt/TiO_2, where x represents the weight percentage of Pt. For the catalyst synthesis of kg-scale reaction, a similar procedure was used for catalyst preparation except that concentrated aqueous hydrogen hexachloroplatinic acid solution (37.7 mg Pt·mL^{-1}, Alfa Aesar) was used.

Preparation of Pt_S/TiO_2

A two-step impregnation method was used to synthesize Pt_S/TiO_2. For a typical catalyst preparation (1.0 g), desired amount of aqueous hydrogen hexachloroplatinic acid solution (7.5 mg Pt·mL^{-1}, Alfa Aesar) and ethylenediamine solution (Pt: ethylenediamine = 1:2 in mol) was diluted to 16 mL in deionized water, and heated in an oil bath to 60 °C with vigorous stirring (800 r.p.m.) for 15 min, followed by the addition of TiO_2 support (P25, Sigma-Aldrich). The temperature was kept at 60 °C for 2 h. After being cooled down, water was removed using rotatory evaporation. The sample was ground thoroughly and then calcined at 300 °C for 3 h with a heating rate of 10 °C·min^{-1}. Then the catalyst was washed with 1 M NH_4Cl, and the resultant material was put into an oven at 110 °C overnight. Finally, the sample was reduced in a flow-tube furnace under a steady flow of 5% H_2/Ar at 300 °C for 3 h with a heating rate of 5 °C·min^{-1}.

Preparation of Pt_L/TiO_2

Sol-immobilization method is used to prepare Pt_L/TiO_2. To initiate the synthesis process, a sol containing Pt NPs was prepared first. The desired amount of H_2PtCl_6 solution was pipetted into the beaker. Subsequently, 28 mL of water was added to the beaker, and the solution was stirred for 5 min. The PVA solution, with a PVA: Pt weight ratio of 1:1, was then added to the beaker, followed by stirring for 20–30 min to form Pt-PVA colloid. To reduce the Pt particle and control its size, a freshly prepared sodium borohydride ($NaBH_4$) solution was added to the mixture. The $NaBH_4$: Pt mole ratio was set at 4:1. The stirrer speed was then increased to 800 r.p.m., and the solution was left to stir for 30 min. Then H_2SO_4 was added to adjust the pH to 3. Subsequently, the desired amount of TiO_2 support was gradually added to the beaker, ensuring the dissolution of any powder on the liquid surface before adding more. The solution was left to stir for 40 min. The catalyst solution was poured into the funnel, with the beaker rinsed using deionized water to ensure complete transfer. The water level in the funnel was maintained during the washing process by adding additional water as needed. After all the water had passed through the funnel, the funnel was placed in an oven (110 °C) overnight.

Diastereoselective hydrogenation of dimethyl phthalate

Unless otherwise stated, reactions were performed in autoclaves. Solvents were used directly without further purification. Gas chromatography (GC) was performed on an HP 6890 with a HP5 column (Agilent). All the materials were tested as catalysts without any further treatment. For a typical small-scale reaction (2 mL) procedure, the

desired amount of catalyst (0.5 mol% of Pt), 0.5 mmol of substrate, and 2 mL of solvent were added in a 4 mL vial with a magnetic stirring bar and septum cap. Then, a needle was inserted in the septum, allowing H_2 to enter the vial. The vials (up to eight) were set in an alloy plate and placed in a 300 mL steel Parr autoclave. The autoclave was flushed with H_2 for times at 10 bar and finally pressurized to 10 bar. Then, it was placed into an aluminum block and kept at 25 °C for 16 h. When the reaction is completed, the autoclave is vented. Finally, the samples were removed from the autoclave with the addition of *n*-hexadecane as the internal standard and ethyl acetate to the crude mixture, followed by filtration to separate the solid catalysts using a celite pad. The organic layer was analyzed at the GC-FID (Agilent 7890 A) and by NMR.

Calculation of TOF

The reaction was performed at three different times (in all cases conversions < 20%). Then we plotted the concentration of the reactant as a function of time. At such a low conversion, the coverage of the product on the catalyst surface was negligible, and we could assume that all the active sites were involved in the reaction. A linear correlation could be obtained by curve fitting. The initial rate (r) was calculated from the slope[57]:

$$r = -\frac{\mathrm{d[R]}}{\mathrm{dt}} = -slope \tag{1}$$

Where r is the initial rate, mol·L^{-1}·h^{-1}; [R] is the concentration of the reactant, mol·L^{-1}; t is the reaction time, h.

The TOF is calculated as follow:

$$TOF = \frac{rV}{n_{Pt}} \tag{2}$$

Where V is the volume of the reaction mixture, L; n_{Pt} is the amount of surface Pt, mol, which is calculated as follow:

$$n_{Pt} = n_{total\ Pt} \times d \tag{3}$$

Where $n_{\mathrm{total\ Pt}}$ is the total amount of Pt in one reaction, mol; d is the dispersion of Pt, determined by CO chemisorption, as shown in Supplementary Table 3.

Each measurement was repeated three times to plot the error bar.

Catalyst recycling

In order to exclude the effect of catalyst loss during the operation procedure, we used two batches of catalysts for recycling tests. In batch A0, we used the standard amount of catalyst. In the second batch, B0, an excess amount of catalyst (*ca.* ten times that of A0) was used. The reaction condition and operation procedure were identical to the hydrogenation reaction. After one hydrogenation reaction, the reaction mixture in batch A0 was analyzed by GC-FID, and the result was recorded as the activity for the fresh catalyst. On the other hand, the catalyst in batch B0 was separated by centrifugation and washed with cyclohexane three times, followed by being dried in an oven at 80 °C for 2 h. Then the catalyst was collected and ground thoroughly, after which it was put into the vacuum line overnight for the complete removal of adsorbed species. For the second run, the standard amount of catalyst was taken out from batch B0 and denoted as batch A1, and the rest was denoted as batch B1. Both batches were set up for reaction. The result of batch A1 was regarded as the activity for the second run. The catalyst in batch B1 was regenerated using the same method above. The procedure was repeated up to five runs of the catalyst.

Kg-scale reaction

Desired amount of catalyst (0.5 mol% of Pt) and *ca.* 250 mL of di-n-octyl phthalate were added into a 450 mL steel Parr autoclave. The reaction proceeded under mechanical stirring. The autoclave was flushed with H_2 three times at 10 bar and finally pressurized to 40 bar. Then, it was placed into an aluminum block and kept at 80 °C. The pressure of H_2 was continuously monitored during the reaction process. When the H_2 pressure decreased below 20 bar, it was recharged to *ca.* 40 bar. When the H_2 pressure remained stable, the reaction was supposed to be completed. The autoclave was vented, and then the solid catalyst and product were separated by filtration. The liquid product was directly collected without purification. The catalyst was washed using cyclohexane, followed by drying in an oven at 80 °C for 2 h. Then the catalyst was collected and ground thoroughly, followed by being put into a vacuum line overnight for the complete removal of adsorbed species. The recycled catalyst was directly used for the next run without any further regeneration procedure. Four cycles were performed in total.

Characterizations

CO chemisorption. CO chemisorption measurements were conducted using a 3-Flex Micromeritics instrument. A 200 mg sample was placed into a U-shaped quartz reactor and heated from room temperature (RT) to 450 °C at a rate of 10 K/min under a flow of 5% O_2/He (50 ml/min), with the temperature maintained for 60 min. The sample was then cooled under an Ar flow (50 ml/min). Following this, the sample was reduced in 5% H_2/Ar (50 ml/min), heated to 200 °C at 5 K/min for 60 min, and further heated to 300 °C (10 K/min) under Ar. After cooling to RT, the sample loop was filled with 20% CO/He, and CO pulses were introduced into the sample using He as the carrier gas (50 ml/min). The resulting peaks were recorded and integrated using a thermal conductivity detector (TCD). The chemisorption stoichiometry was assumed to be Pt_{surf}: CO = 1:1, and a spherical metal particle shape was considered for calculations.

XPS

The XPS measurements were performed on an ESCALAB 220iXL (Thermo Fisher Scientific) with monochromated Al Kα radiation (E = 1486.6 eV). Samples are prepared on a stainless-steel holder with conductive double-sided adhesive carbon tape. The measurements are performed with charge compensation using a flood electron system combining low-energy electrons and Ar^+ ions ($p_{Ar} = 1 \times 10^{-7}$ mbar). The electron binding energies are referenced to the C 1s core level of carbon at 284.8 eV (C-C and C-H bonds). For quantitative analysis, the peaks were deconvoluted with Gaussian-Lorentzian curves using the software Unifit 2023. The peak areas were normalized by the transmission function of the spectrometer and the element-specific sensitivity factor of Scofield.

STEM

The morphology and particle size/structure of Pt-loaded catalysts were characterized using a Thermo Fisher Spectra 300 scanning transmission electron microscope equipped with a high-angle annular dark field (HAADF) detector and a Cs probe corrector (CEOS), operating at 300 kV. The TEM samples were prepared by dispersing the catalyst powders into a methanol solution, followed by sonication and drop-casting the solution onto a copper grid coated with an amorphous holey carbon film. The particle size distribution was analyzed from HAADF electron micrographs using the ImageJ software package[58]. To make the analysis representative, we counted *ca.* 500 particles for each sample.

Nuclear magnetic resonance (NMR)

NMR spectra were recorded on Bruker AV 300 spectrometers. All chemical shifts (δ) are reported in parts per million (ppm) and coupling constants (J) in Hz. All chemical shifts are reported relative to the peaks deuterated solvent (e.g., with respect to $CDCl_3$, δ (ppm) = 7.26 for ^{1}H NMR and δ (ppm) = 77.16 for ^{13}C NMR, respectively).

DFT calculations

All spin-polarized calculations were performed using the Vienna Ab initio Simulation Package (VASP, Version 6.4.2)[59], and the generalized gradient approximation with Perdew–Burke–Ernzerhof (GGA-PBE) functional[60,61] was employed to describe the exchange and correlation energies of electrons. The interaction between ion and valence electrons was described using projector-augmented wave (PAW)[62] potential. The energy cutoff for plane wave was set to 400 eV with the convergence criteria of 1×10^{-4} eV/atom and 0.03 eV/Å for energy and max force in all structure optimizations and frequency calculations. The Brillouin zone was sampled with the Monkhorst–Pack method[63].

To understand the activity for catalysts of different sizes at the atomic level, supported Pt_{13} and Pt_{55} nanoclusters on the (3 × 3) and (3 × 4) anatase-TiO_2(101) surfaces were used to simulate the one-shell and two-shell structures, respectively. Besides, the Pt_{159} nanoparticle and the plain Pt(111) facet with a (8 × 8) supercell were constructed to simulate the structure of a three-shell and even larger surface size. All TiO_2(101) surfaces were constructed with a six-atomic-layer thickness, where the bottom three layers were fixed in their bulk positions, and the others were relaxed. A vacuum region of at least 15 Å was set for all surface models to avoid the perpendicular interactions with adjacent slabs in the Z-direction, and an effective Hubbard parameter (U_{eff})[64] of 4.0 eV was set for Ti-3d states. The k-points for Pt_{13}/TiO_2(101), Pt_{55}/TiO_2(101), Pt_{159}, Pt(111) models were setting to 3 × 3 × 1, 2 × 2 × 1, 2 × 2 × 1 and 2 × 2 × 1, respectively.

The adsorption energy (E_{ads}) for the reactant was computed according to the equation, $E_{ads} = E_{X/slab} - E_X - E_{slab}$, where the $E_{X/slab}$, E_X, and E_{slab} are the total optimized energy for the adsorbed configurations, isolated species, and bare slab, respectively.

Data availability

All data are available from the corresponding author upon request. All original data needed to evaluate the conclusions in the paper are already present in the manuscript and the Supplementary Information.

References

1. Lückemeier, L., Pierau, M. & Glorius, F. Asymmetric arene hydrogenation: towards sustainability and application. *Chem. Soc. Rev.* **52**, 4996–5012 (2023).
2. Hu, Y. et al. Efficient synthesis of novel plasticizers by direct palladium-catalyzed Di- or multi-carbonylations. *Angew. Chem. Int. Ed.* **62**, e202214706 (2023).
3. Petrukhina, N. N., Vinnikova, M. A. & Maksimov, A. L. Production of high-density jet and diesel fuels by hydrogenation of highly aromatic fractions. *Russ. J. Appl. Chem.* **91**, 1223–1254 (2018).
4. Jorschick, H., Preuster, P., Bösmann, A. & Wasserscheid, P. Hydrogenation of aromatic and heteroaromatic compounds—a key process for future logistics of green hydrogen using liquid organic hydrogen carrier systems. *Sustain. Energy Fuels* **5**, 1311–1346 (2021).
5. Wei, D. et al. Toward a hydrogen economy: development of heterogeneous catalysts for chemical hydrogen storage and release reactions. *ACS Energy Lett.* **7**, 3734–3752 (2022).
6. Fuller, N. et al. An improved model for fragment-based lead generation at AstraZeneca. *Drug Discov. Today* **21**, 1272–1283 (2016).
7. Scott, K. A., Cox, P. B. & Njardarson, J. T. Phenols in pharmaceuticals: analysis of a recurring motif. *J. Med. Chem.* **65**, 7044–7072 (2022).
8. Hamilton, D. J. et al. Escape from planarity in fragment-based drug discovery: a physicochemical and 3D property analysis of synthetic 3D fragment libraries. *Drug Discov. Today Technol* **38**, 77–90 (2020).
9. Lovering, F., Bikker, J. & Humblet, C. Escape from flatland: increasing saturation as an approach to improving clinical success. *J. Med. Chem.* **52**, 6752–6756 (2009).
10. Zhang, Z., Butt, N. A. & Zhang, W. Asymmetric hydrogenation of nonaromatic cyclic substrates. *Chem. Rev.* **116**, 14769–14827 (2016).
11. Bourriquen, F. et al. Diastereoselective hydrogenation of arenes and pyridines using supported ruthenium nanoparticles under mild conditions. *Chem. Commun.* **58**, 8842–8845 (2022).
12. Kistiakowsky, G. B., Ruhoff, J. R., Smith, H. A. & Vaughan, W. E. Heats of organic reactions. IV. Hydrogenation of some dienes and of benzene. *J. Am. Chem. Soc.* **58**, 146–153 (1936).
13. Clarke, J. J., Maekawa, Y., Nambo, M. & Crudden, C. M. Borenium-catalyzed reduction of pyridines through the combined action of hydrogen and hydrosilane. *Org. Lett.* **23**, 6617–6621 (2021).
14. Zhou, Q. et al. Borane-catalyzed transfer hydrogenations of pyridines with ammonia borane. *Org. Lett.* **18**, 5189–5191 (2016).
15. Liu, Y. & Du, H. Metal-free borane-catalyzed highly stereoselective hydrogenation of pyridines. *J. Am. Chem. Soc.* **135**, 12968–12971 (2013).
16. Kim, A. N. et al. Iridium-catalyzed enantioselective and diastereoselective hydrogenation of 1,3-disubstituted isoquinolines. *ACS Catal.* **10**, 3241–3248 (2020).
17. Kim, S., Loose, F., Bezdek, M. J., Wang, X. & Chirik, P. J. Hydrogenation of N-heteroarenes using rhodium precatalysts: reductive elimination leads to formation of multimetallic clusters. *J. Am. Chem. Soc.* **141**, 17900–17908 (2019).
18. Wiesenfeldt, M. P., Nairoukh, Z., Li, W. & Glorius, F. Hydrogenation of fluoroarenes: Direct access to all-*cis*-(multi)fluorinated cycloalkanes. *Science* **357**, 908–912 (2017).
19. Nairoukh, Z., Wollenburg, M., Schlepphorst, C., Bergander, K. & Glorius, F. The formation of all-cis-(multi)fluorinated piperidines by a dearomatization–hydrogenation process. *Nat. Chem.* **11**, 264–270 (2019).
20. Kaithal, A. et al. Access to unexplored 3D chemical space: *cis*-selective arene hydrogenation for the synthesis of saturated cyclic boronic acids. *Angew. Chem. Int. Ed.* **61**, e202206687 (2022).
21. Stalzer, M. M. et al. Single-face/All-cis arene hydrogenation by a supported single-site d0 organozirconium catalyst. *Angew. Chem. Int. Ed.* **55**, 5263–5267 (2016).
22. Joannou, M. V., Bezdek, M. J. & Chirik, P. J. Pyridine(diimine) molybdenum-catalyzed hydrogenation of arenes and hindered olefins: insights into precatalyst activation and deactivation pathways. *ACS Catal.* **8**, 5276–5285 (2018).
23. Widegren, J. A. & Finke, R. G. A review of soluble transition-metal nanoclusters as arene hydrogenation catalysts. *J. Mol. Catal. A Chem.* **191**, 187–207 (2003).
24. Wang, R., Zhang, M., Zhang, J. & Yang, J.-H. Supported nickel-based catalysts for heterogeneous hydrogenation of aromatics. *ChemistrySelect* **8**, e202302787 (2023).
25. Qi, S.-C., Wei, X.-Y., Zong, Z.-M. & Wang, Y.-K. Application of supported metallic catalysts in catalytic hydrogenation of arenes. *RSC Adv.* **3**, 14219–14232 (2013).
26. Chacón, G. & Dupont, J. Arene hydrogenation by metal nanoparticles in ionic liquids. *ChemCatChem* **11**, 333–341 (2019).
27. Glorius, F., Spielkamp, N., Holle, S., Goddard, R. & Lehmann, C. W. Efficient asymmetric hydrogenation of pyridines. *Angew. Chem. Int. Ed.* **43**, 2850–2852 (2004).
28. Heitbaum, M., Fröhlich, R. & Glorius, F. Diastereoselective hydrogenation of substituted quinolines to enantiomerically pure decahydroquinolines. *Adv. Synth. Catal.* **352**, 357–362 (2010).
29. Miyamura, H. & Kobayashi, S. Reaction rate acceleration of cooperative catalytic systems: metal nanoparticles and Lewis acids in arene hydrogenation. *Angew. Chem. Int. Ed.* **61**, e202201203 (2022).
30. Yamamoto, H., Noda, K., Horiguti, H. & Kwan, T. Stereoselective hydrogenation of o-, m-, and p-xylenes by transition metal catalysts of group VIII. *Chem. Pharm. Bull.* **15**, 752–755 (1967).

31. Qu, R., Junge, K. & Beller, M. Hydrogenation of carboxylic acids, esters, and related compounds over heterogeneous catalysts: a step toward sustainable and carbon-neutral processes. *Chem. Rev.* **123**, 1103–1165 (2023).
32. Macino, M. et al. Tuning of catalytic sites in Pt/TiO_2 catalysts for the chemoselective hydrogenation of 3-nitrostyrene. *Nat. Catal.* **2**, 873–881 (2019).
33. Lin, S. D. & Vannice, M. A. Hydrogenation of aromatic hydrocarbons over supported Pt catalysts.I. Benzene hydrogenation. *J. Catal.* **143**, 539–553 (1993).
34. Bratlie, K. M., Kliewer, C. J. & Somorjai, G. A. Structure effects of benzene hydrogenation studied with sum frequency generation vibrational spectroscopy and kinetics on Pt(111) and Pt(100) single-crystal surfaces. *J. Phys. Chem. B* **110**, 17925–17930 (2006).
35. Lin, S. D. & Vannice, M. A. Hydrogenation of aromatic hydrocarbons over supported Pt catalysts.III. Reaction models for metal surfaces and acidic sites on oxide supports. *J. Catal.* **143**, 563–572 (1993).
36. Guo, M., Kong, X., Li, C. & Yang, Q. Hydrogenation of benzoic acid derivatives over Pt/TiO_2 under mild conditions. *Commun. Chem.* **4**, 54 (2021).
37. Pushkarev, V. V., An, K., Alayoglu, S., Beaumont, S. K. & Somorjai, G. A. Hydrogenation of benzene and toluene over size controlled Pt/SBA-15 catalysts: elucidation of the Pt particle size effect on reaction kinetics. *J. Catal.* **292**, 64–72 (2012).
38. Liu, L. & Corma, A. Metal catalysts for heterogeneous catalysis: from single atoms to nanoclusters and nanoparticles. *Chem. Rev.* **118**, 4981–5079 (2018).
39. Koussathana, M., Vamvouka, D., Economou, H. & Verykios, X. Slurry-phase hydrogenation of aromatic compounds over supported noble metal catalysts. *Appl. Catal.* **77**, 283–301 (1991).
40. Aksoylu, A. E., Madalena, M., Freitas, A., Pereira, M. F. R. & Figueiredo, J. L. The effects of different activated carbon supports and support modifications on the properties of Pt/AC catalysts. *Carbon* **39**, 175–185 (2001).
41. Vieira, M. G. A., Da Silva, M. A., Dos Santos, L. O. & Beppu, M. M. Natural-based plasticizers and biopolymer films: a review. *Eur. Polym. J.* **47**, 254–263 (2011).
42. Wang, Y. & Qian, H. Phthalates and their impacts on human health. *Healthcare* **9**, 603 (2021).
43. Swann, W. A., Yadav, A., Colvin, N. B., Freundl, N. K. & Li, C. W. Diastereoselective hydrogenation of tetrasubstituted olefins using a heterogeneous Pt–Ni alloy catalyst. *Angew. Chem. Int. Ed* **63**, e202317710 (2024).
44. Gunasekar, R., Goodyear, R. L., Proietti Silvestri, I. & Xiao, J. Recent developments in enantio- and diastereoselective hydrogenation of *N*-heteroaromatic compounds. *Org. Biomol. Chem.* **20**, 1794–1827 (2022).
45. Wiesenfeldt, M. P., Nairoukh, Z., Dalton, T. & Glorius, F. Selective arene hydrogenation for direct access to saturated carbo- and heterocycles. *Angew. Chem. Int. Ed.* **58**, 10460–10476 (2019).
46. Yang, J. et al. syn-Selective construction of fused heterocycles by catalytic reductive tandem functionalization of n-heteroarenes. *ACS Catal* **11**, 9271–9278 (2021).
47. Wang, D.-S., Chen, Q.-A., Lu, S.-M. & Zhou, Y.-G. Asymmetric hydrogenation of heteroarenes and arenes. *Chem. Rev.* **112**, 2557–2590 (2012).
48. Kim, A. N. & Stoltz, B. M. Recent advances in homogeneous catalysts for the asymmetric hydrogenation of heteroarenes. *ACS Catal* **10**, 13834–13851 (2020).
49. Williams, S., Qi, L., Cox, R. J., Kumar, P. & Xiao, J. Hydrogenation of functionalised pyridines with a rhodium oxide catalyst under mild conditions. *Org. Biomol. Chem.* **22**, 1010–1017 (2024).
50. Chhabra, A., Reich, S., Shannon, T. M., Maleczka, R. E. Jr & Smith, I. I. I. M. R. Access to $C(sp^3)$ borylated and silylated cyclic molecules: hydrogenation of corresponding arenes and heteroarenes. *RSC Adv.* **14**, 10590–10607 (2024).
51. Duan, L., Wang, L., Yao, G., Zhu, X., Sun, Y., Lv, F., Liu, H., Yang, Y., Li, L., Luo, Y. & Wan, Y. A d-electron deficient Pd trimer for exceptional pyridine hydrogenation activity and selectivity. *Angew. Chem. Int. Ed.* **64**, e202503926 (2025).
52. Li, Y., Wang, A., Shen, Y. & Zhang, P. Convenient enzymatic resolution of cis-6-benzyltetrahydro-1H-pyrrolo [3, 4-b] pyridine-5, 7 (6H, 7aH)-dione using lipase to prepare the intermediate of moxifloxacin. *J. Mol. Catal. B Enzym.* **110**, 178–183 (2014).
53. Dhiman, P., Arora, N., Thanikachalam, P. V. & Monga, V. Recent advances in the synthetic and medicinal perspective of quinolones: a review. *Bioorg. Chem.* **92**, 103291 (2019).
54. Reddy, G. P. & Bandichhor, R. A novel synthesis of (4aS, 7aS)-octahydro-1H-pyrrolo [3, 4-b] pyridine: an intermediate of moxifloxacin hydrochloride. *Asian J. Chem.* **25**, 8701 (2013).
55. Fabro, S., Schumacher, H., Smith, R., Stagg, R. & Williams, R. The metabolism of thalidomide: some biological effects of thalidomide and its metabolites. *Br. J. Pharmacol. Chemother.* **25**, 352 (1965).
56. Lepper, E. R., Smith, N. F., Cox, M. C., Scripture, C. D. & Figg, W. D. Thalidomide metabolism and hydrolysis: mechanisms and implications. *Curr. Drug Metab.* **7**, 677–685 (2006).
57. Kozuch, S. & Martin, J. M. L. "Turning Over" definitions in catalytic cycles. *ACS Catal.* **2**, 2787–2794 (2012).
58. Schneider, C. A., Rasband, W. S. & Eliceiri, K. W. NIH image to ImageJ: 25 years of image analysis. *Nat. Methods* **9**, 671–675 (2012).
59. Kresse, G. & Furthmüller, J. Efficient iterative schemes for ab initio total-energy calculations using a plane-wave basis set. *Phys. Rev. B* **54**, 11169–11186 (1996).
60. Perdew, J. P., Burke, K. & Ernzerhof, M. Generalized gradient approximation made simple. *Phys. Rev. Lett.* **77**, 3865–3868 (1996).
61. Ernzerhof, M. & Scuseria, G. E. Assessment of the Perdew–Burke–Ernzerhof exchange-correlation functional. *J. Chem. Phys.* **110**, 5029–5036 (1999).
62. Blöchl, P. E. Projector augmented-wave method. *Phys. Rev. B* **50**, 17953–17979 (1994).
63. Pack, J. D. & Monkhorst, H. J. "Special points for Brillouin-zone integrations"—a reply. *Phys. Rev. B* **16**, 1748–1749 (1977).
64. Vladimir, I. A., Aryasetiawan, F. & Lichtenstein, A. I. First-principles calculations of the electronic structure and spectra of strongly correlated systems: the LDA + U method. *J. Phys. Condens. Matter* **9**, 767 (1997).

Acknowledgements

We thank the analytical staff of the Leibniz Institute for Catalysis for their excellent service. We thank the support of the Carbon Neutrality and Energy System Transformation (CNEST) Program. R.Q. gratefully acknowledges the financial support from the Alexander von Humboldt Foundation (CHN 1212814 HFST-P). LX and HY acknowledge the China Scholarship Council for the financial support.

Author contributions

R.Q., S.J., L.X., and H.Y. contributed equally. R.Q. conceived the idea for the catalyst design and optimization. R.Q. and L.X. prepared the catalysts. R.Q. performed the kinetic studies and analyzed the data. S.J. optimized conditions for the substrate scope and carried out the application studies. R.Q., L.X., and R.C. were responsible for the electron microscopy studies and corresponding data analysis; R.Q., S.J., R.J., and R.F. performed the kg-scale tests. S.B. carried out XPS measurements. H.A. worked on the CO chemisorption measurement. H.Y. performed the DFT calculations under the supervision of H.J. K.J., H.J., G.J.H., and M.B. Supervised the research activities, provided guidance for synthetic applications, and supported the project with funding acquisition; R.Q., S.J., K.J., and M.B. co-wrote the paper; all the authors contributed to editing the manuscript.

Competing interests

R.Q., S.J., R.J., R.F., K.J., and M.B. are the authors of a filed patent on the catalyst system under EP 23215244. The authors declare no other competing interests.

Additional information

Supplementary information The online version contains supplementary material available at https://doi.org/10.1038/s41467-026-68537-7.

Correspondence and requests for materials should be addressed to Kathrin Junge, Haijun Jiao, Graham J. Hutchings or Matthias Beller.

Peer review information *Nature Communications* thanks the anonymous reviewers for their contribution to the peer review of this work. A peer review file is available.